True 3D Land CSAMT Modeling

W. Soyer[1] and R.L. Mackie[1]

[1]CGG Multiphysics
Wolfgang.Soyer@cgg.com
Randall.Mackie@cgg.com

SUMMARY

Controlled source audio magnetotellurics “CSAMT” is a grounded electromagnetic imaging technique used primarily in the mining industry and is a closely related predecessor to the marine controlled source electromagnetic method “CSEM” more familiar to the oil and gas community. Both methods involve injecting alternating electric current into the Earth through long transmitter dipoles, and making measurements of the Earth’s response at an array of EM receivers. Historically, CSAMT data have been interpreted using readily available MT modeling algorithms, but this means using only the data considered far enough away from the dipole source to be interpretable using the MT-inherent assumption of a uniform, or “far-field”, source. In this work, we show the advantages of carrying out complete earth, three-dimensional modeling of all grounded dipole EM fields, including those near the source, and avoiding the commonly employed, ad-hoc methods that throw away otherwise valuable “transition-zone” data that are unusable in MT-only modeling workflows. The CSEM inversion modeling is applied to a synthetic and a real data example, and inversion of complex field amplitudes is compared with impedance inversions.

Keywords: 3D inversion, true layout, CSEM, CSAMT, MT

INTRODUCTION

Controlled source, grounded electrode EM surveys have a long and successful history in mineral exploration geophysics, where the most commonly deployed configuration is CSAMT, using single, fixed, kilometer-long transmitter dipoles in broadside configuration (e.g., Zonge and Hughes 1991). More recently, however, hybrid survey configurations are gaining in popularity, including surveys using multiple transmitter and receiver dipole locations and orientations (e.g., Grayver et al. 2014, Darnet et al. 2018).

Despite continuous advancements in computing power and algorithms, the analysis and modeling of CSAMT data is still generally restricted to “far-field” data, where the standard magnetotelluric (MT) uniform source field assumption is valid, and readily available MT modeling tools are employed (e.g., Sasaki et al, 1992, Wannamaker, 1997). In general, far-field conditions are met at higher frequencies and longer source-receiver offsets. This restriction not only limits the depth of exploration, but also removes the potentially beneficial sensitivity characteristics of EM fields in the transition zone between near-field and far-field behavior, where vertical current components are sensitive to thin resistive layers otherwise invisible to MT. While three-dimensional inversion modeling of land CSAMT is being developed (e.g., Lin et al 2018, Wang et al 2018) it is not yet the industry standard that 3D inversion modeling is for land and marine MT, and marine CSEM.

3D CSEM IMPLEMENTATION

Here we discuss extensions of electromagnetic modeling algorithms (Mackie et al, 2020) for generic, land CSEM array data, including CSAMT configurations. The objective is to provide accurate and efficient modeling of the typically km-long grounded transmitter dipoles, with rugged topography and realistic geology at both receiver and transmitter array locations. We model EM fields using a staggered grid, finite difference technique which is a subset of the more general Finite Integration Technique. In our modeling code, long grounded dipoles are draped over topography. We can model and invert far-field, transition zone, and near-field data in a single workflow, as complete controlled source EM data.

Code verification was carried out using a sequence of 1D models of increasing complexity and comparing 3D results to those obtained with analytical 1D CSEM codes (not shown here). This confirmed that with reasonable gridding we can obtain accuracies to better than 2%, in line with typical finite difference numerical solutions.

SYNTHETIC EXAMPLE

We designed a test 3D model using real topography with about 800m relief (Figure 1). The 3D model has a background resistivity of 100 Ωm and hosts two pairs of 3200×2800×500 m anomalies of 10 Ωm and 5000 Ωm, respectively, draped below 1000m depth (Figure 1). Two perpendicular transmitter orientations were modeled. Receivers were spaced every 400 m, and offsets to the transmitter ranged from 3 km to 12 km. We modeled CSEM forward responses at 28 frequencies from 0.2 Hz to 500 Hz, using all components.

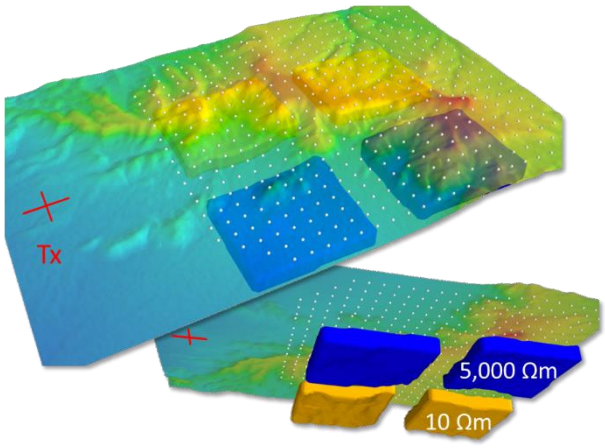

Figure 1. Setup of CSAMT simulated array over topography. The transmitter location (red cross) is to the west at 3 km from closest receivers. The four anomalous 500m thick bodies inserted at 1km below the surface are shown in orange and blue.

Figure 2 shows results from a number of 3D inversions of complex field amplitudes, all of which started from the background resistivity and used low structural regularization. Prior to the inversions we added 1.5% random Gaussian noise to the electric and magnetic fields of the CSEM data. Both the electric broadside data (top row) and the combined electric (scalar) broadside and inline data inversion (middle row) reveal the resistivity structure reasonably well, however the inversion involving the inline component resolves the resistor closer to the transmitter better due to the stronger vertical current flow in this configuration (Figure 3). Magnetic field inversions yield only a very smooth representation of the resistivity structure (Figure 2, bottom).

A question being discussed is whether field amplitude inversions have an advantage over impedance inversions (Routh and Oldenburg 2000). Here we have carried out an impedance inversion for the synthetic broadside setup, and these resulted in higher structural detail than the inversion of the corresponding electric field amplitudes, resulting in better impedance data fits (Figures 4 and 5).

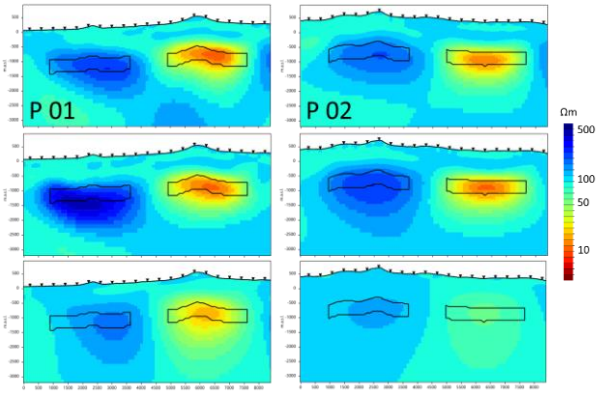

Figure 2. 3D CSEM field inversion results. Data input: top) broadside electric fields; middle) broadside & inline electric fields; bottom) broadside & inline magnetic fields.

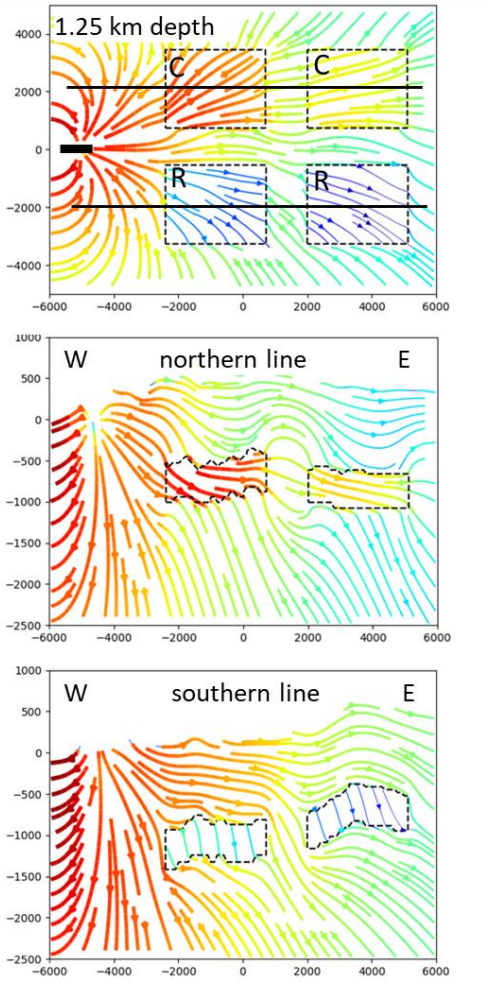

Figure 3. 3D current density for the transmitter in the inline configuration, at 0.2 Hz. Top: depth slice at 1.25km below surface; middle and bottom: cross sections, vertical exaggeration is 2.5. Warm colors and thicker lines mark higher current density.

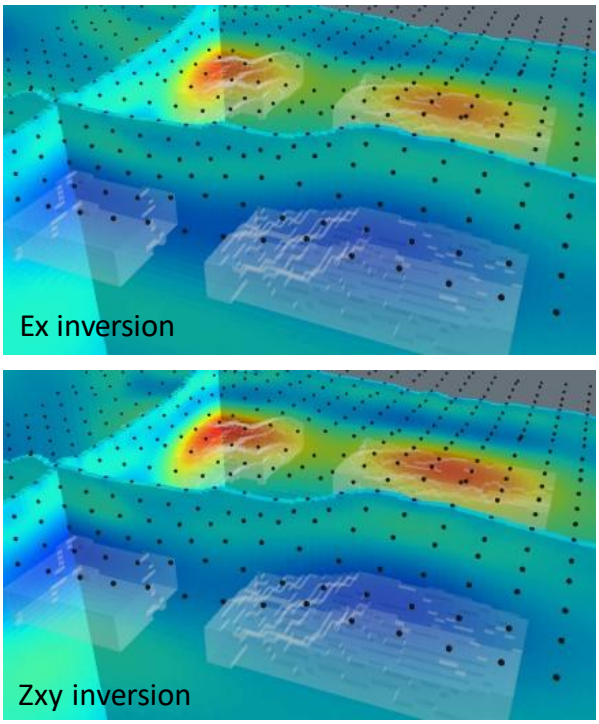

Figure 4. 3D CSEM electric field amplitude inversion (top) compared to the sharper 3D CSEM impedance inversion (bottom). Broadside data were used in both cases.

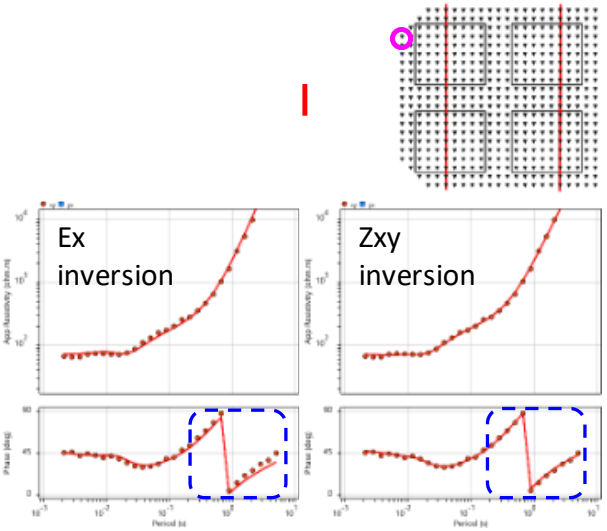

Figure 5. Impedance data fit at high angle from transmitter axis for electric field amplitude (Ex, left) and impedance (Zxy, right) 3D CSEM inversion. The impedance inversion achieves a better fit, as might be expected, as magnetic fields are not inverted in the Ex only inversion.

REAL DATA EXAMPLE - SILVERBELL

We applied our new inversion algorithm to a 1993 CSAMT legacy data set from the Silverbell mine in Arizona. Line and site spacing is 240m and 60m, respectively, and other geometric parameters are shown in Figure 6.

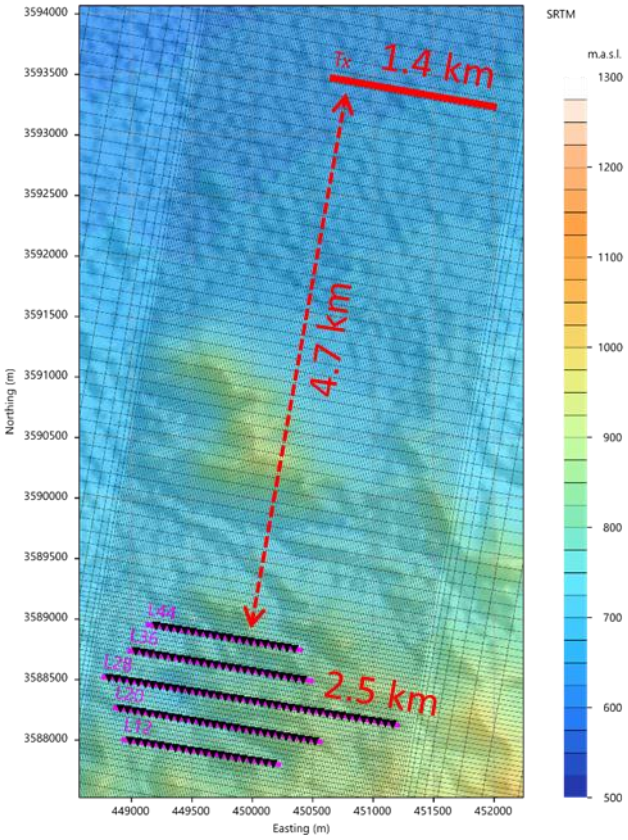

Figure 6. Scalar, broadside CSAMT survey at Silverbell. Transmitter-receiver distance is >4.7 km.

A 3D mesh was created with 20x60x10 m spacing in the topographic core, and a wider 100m crossline spacing between the transmitter and the receivers (1.5 million cells total). Input data for 3D CSEM inversions were scalar impedances at all 9 frequencies between 32 Hz and 8192 Hz. A homogeneous 150 Ωm was used as starting model.

The 3D CSEM inversion gives a good data fit across the full frequency range (Figure 7). Results are shown along line L28 in Figure 8 (bottom) in comparison with 1D and 2D MT inversions (TM-mode data). The 3D inversion provides a smooth image, without strong imprint from statics.

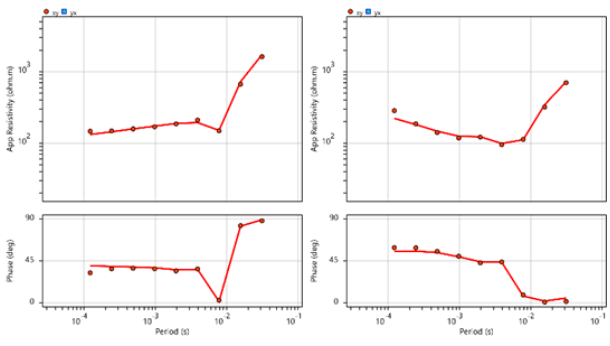

Figure 7. Data fit examples from 3D CSEM inversion impedance inversion at Silverbell.

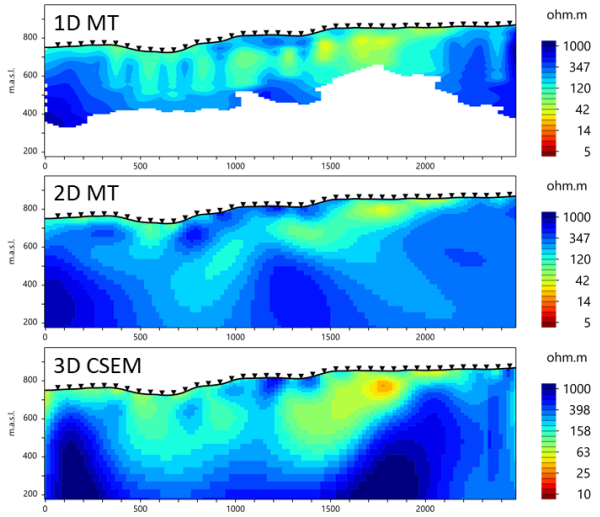

Figure 8. Comparison between 1D & 2D MT, and 3D CSEM impedance inversion, along line L28. Input data to MT TM-mode inversions excluded the lowest three frequencies. 1D inversions are affected by statics.

The 3D CSEM results also match well with earlier published 2D results (comparison not shown here). Note the Silverbell mine has evolved dramatically since the acquisition of this data set.

Conclusions

We have extended our land, marine and airborne 3D EM inversion modeling algorithms to include generic land controlled-source EM modeling. While we can now model any arbitrary set up of transmitter and receiver dipole orientations and locations, here we have concentrated on the typical CSAMT field deployment with one or two long grounded transmitter and an array of receivers at a certain offset. True controlled source inversion of the CSEM data results in good recovery of resistivity anomalies for the synthetic setup, especially when inverting impedances or inverting electric field data from two polarizations. An additional benefit is the ability to model all data from near-field through the transition zone and into the far-field, eliminating ad hoc methods to remove near-field and transition zone data.

Acknowledgements

We would like to thank Scott Urquhart and Scott McInnes from Zonge Intl. for providing the Silverbell data. We highly appreciate the sharing of industry insight by these and additionally Simon Mann (Zonge Australia), Roger Sharpe (Quantec) and Yann Avram (Phoenix).

References

Darnet M, Wawrzyniak P, Coppo N, Nielsson S, Schill E, Fridleifsson GO (2018) Monitoring geothermal reservoir developments with the Controlled-Source Electro-Magnetic method – A calibration study on the Reykjanes geothermal field: Journal of Volcanology and Geothermal Research: 391, doi:10.1016/j.jvolgeores.2018.08.015.

Grayver AV, Streich R, Ritter O (2014) 3D inversion and resolution analysis of land-based CSEM data from the Ketzin CO2 storage formation: Geophysics 79(2): E101–E114, doi:10.1190/Geo2013-0184.1.

Lin C, Zhong S, Auken E, Cai H, Tan H, Peng M, Kong W (2018) The effects of 3D topography on controlled-source audio-frequency magnetotelluric responses. Geophysics 83(2): WB97–108.

Mackie RL, Meju MA, Miorelli F, Miller RV, Scholl C, Shahir AS (2020), Seismic image-guided 3D inversion of marine controlled-source electromagnetic and magnetotelluric data. Interpretation 8: SS1-SS13.

Routh PS, Oldenburg, DW (2000) Advantages of field component inversion of CSAMT data, SEG Tech Program Expand Abstr doi:10.1190/1.1815997.

Sasaki Y, Yoshihiro Y, Matsuo K (1992) Resistivity imaging of controlled-source audiofrequency magnetotelluric data. Geophysics 57: 952-955.

Wang T, Wang K, Tan H (2017) Forward modeling and inversion of tensor CSAMT in 3D anisotropic media. Applied Geophysics 14: 590–605, doi:10.1007/s11770-017-0644-7.

Wannamaker P (1997) Tensor CSAMT survey over the Sulphur Springs thermal area, Valles Caldera, New Mexico, Part I: Implications for structure of the western caldera / Part II: Implications for CSAMT methodology: Geophysics 62: 451-465 / 466-476.

Zonge KL, Hughes LJ (1991) Controlled source audio-frequency magnetotellurics, in M. N. Nabighian, ed., Electromagnetic Methods in Applied Geophysics 2b: 713-809, Soc. Expl. Geophys, Tulsa